Available online at www.sciencedirect.com
SCIENCE DIRECT®
International Journal of Multiphase Flow 31 (2005) 1–24
International Journal of Multiphase Flow
www.elsevier.com/locate/ijmulflow

Gas entrainment by a liquid film falling around a stationary Taylor bubble in a vertical tube

J.P. Kockx, F.T.M. Nieuwstadt, R.V.A. Oliemans [1], R. Delfos *

J.M. Burgers Centre, Delft University of Technology, Lab. for Aero- and Hydrodynamics, Leeghwaterstraat 21, 2628 CA Delft, The Netherlands

Received 24 July 2002; received in revised form 20 August 2004

Abstract

Gas entrainment by a liquid film falling around a stationary Taylor bubble in a 0.1 m diameter vertical tube is studied experimentally with the purpose of validating a model formulated in an earlier phase of our research. According to this model for a fixed liquid velocity the gas entrainment should be proportional to the waviness of the film (its intermittency) and the wave height and inversely proportional to the film thickness. For Taylor bubble lengths ranging from $1D$ to $15D$ these film parameters have been measured with a Laser Induced Fluorescence technique. The gas entrainment has been determined from the net gas flux into the liquid column underneath the Taylor bubble by using data on gas re-coalescence into the rear of the Taylor bubble. These data are available for lengths ranging from $4.5D$ to $9D$. The model results with the measured film characteristics compare well with the observed gas entrainment. The fact that the net gas flux becomes constant for long Taylor bubbles, whereas the wave height still increases, warrants further study.

Keywords: Slug flow; Taylor bubble; Liquid film; Entrainment; Laser induced fluorescence; Wave height

* Corresponding author. Tel.: +31 15 2782963; fax: +31 15 2782947.
E-mail address: r.delfos@wbmt.tudelft.nl (R. Delfos).
[1] Present address: Kramers Lab. voor Fysische Technologie Prins Bernhardlaan 6, 2628 BW Delft, The Netherlands.

0301-9322/$ - see front matter © 2004 Elsevier Ltd. All rights reserved.
doi:10.1016/j.ijmultiphaseflow.2004.08.005

1. Introduction

Liquid–gas flow in a vertical pipe is one of the fundamental flows in the field of two-phase flow. Depending on the flow rates of the gas and liquid, the flow patterns in this case can differ considerably. Four distinct flow patterns are in general distinguished, which for increasing gas-flow rates are bubbly flow, slug flow, churn flow and annular flow. Here we concentrate on slug flow.

Slug flow is characterised by a liquid flow in combination with a series of large axis-symmetric bullet-shaped gas bubbles, the so-called Taylor bubbles. These bubbles occupy most of the cross-section of the pipe and move upward much faster than the liquid. Between the Taylor bubble and the tube wall the liquid flows downwards as a thin free-falling film (assuming that the mixture velocity is not too high). The Taylor bubbles are separated by regions of continuous liquid phase that contain small gas bubbles. These regions are denoted as liquid slugs. A schematic picture of a vertical slug flow is given in Fig. 1.

Vertical slug flow is encountered in many industrial two-phase flow applications. For instance, it occurs during oil production and in the flows occurring in various process equipment. Slug flow can also be encountered in daily life. An example is a coffee-maker, where the slug bubbles are used to pump the water up towards the coffee filter.

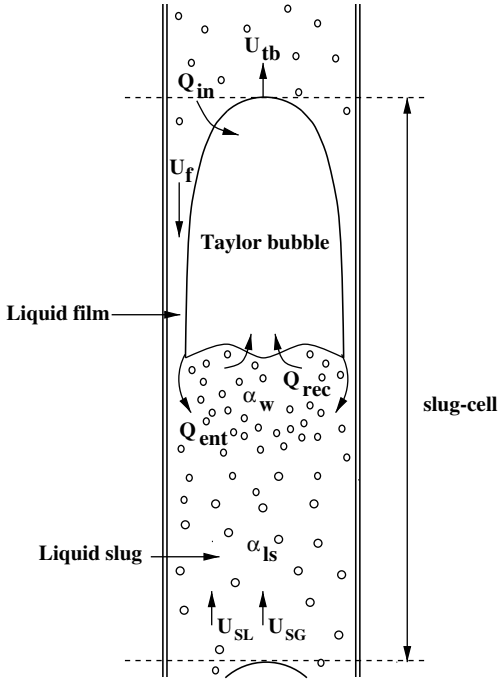

Fig. 1. A schematic picture of one slug-cell in a vertical slug flow. A slug-cell consists of a Taylor bubble and the following liquid slug. Q_{in}, Q_{ent} and Q_{rec} are the gas in-flux, entrainment and re-coalescence gas flux, respectively. U_{tb} and U_f are the velocity of the Taylor bubble and the film velocity. U_{SL} and U_{SG} are the superficial liquid and gas velocity, respectively. α_{ls} is the void fraction in the liquid slug and α_w the gas fraction in the wake of the Taylor bubble.

The strongly instationary flow conditions during slug flow may have a large mechanical impact on the equipment in which this flow occurs. For industrial applications it is therefore important to determine the conditions for which slug flow can appear and particularly to predict the void fraction of the flow. For this different models have been proposed and measurements have been done (Fernandes et al., 1983; Brauner and Barnea, 1985, Orell and Rembrandt, 1986; Fabre and Liné, 1992; Shemer and Barnea, 1989; van Hout et al., 1992). These models are based on the assumption of a fully developed (steady) slug flow, where the Taylor bubbles and liquid slugs rise steadily and follow each other at a constant distance. In that case we can consider the flow as a train of so-called slug-cells, each consisting of one Taylor bubble together with the surrounding liquid film and one successive liquid slug. Such a slug-cell is indicated in Fig. 1.

In their model, based on a description in terms of a slug cell, Fernandes et al. (1983) predict the void fraction in the liquid slug by considering the gas fluxes into and out of the Taylor bubble. When the liquid flows around the nose of the Taylor bubble it deforms into a film too thin to accommodate the bubbles carried within liquid slug (assuming a low-viscous liquid). As a result these bubbles coalesce with the nose of the Taylor bubble, which results in a gas flow rate into the Taylor bubble, indicated as Q_{in} in Fig. 1. At the bottom of the Taylor bubble small bubbles are torn off due to the falling film which plunges into the liquid slug. This gas flow rate out of the Taylor bubble is indicated as the entrainment flux, Q_{ent} in Fig. 1. A part of these entrained gas bubbles re-coalesces back into the Taylor bubble at its trailing edge, which results in a re-coalescence flux Q_{rec}. The material balance for a stationary Taylor bubble requires that

$$Q_{ent} = Q_{in} + Q_{rec}. \tag{1}$$

The net gas flux out of the rear of the Taylor bubble is the entrainment flux minus the re-coalescence flux. For the case of a stationary Taylor bubble this net flux out of the bottom of the Taylor bubble should, according to Eq. (1), be equal to the gas flux into the Taylor bubble, Q_{in}, so that

$$Q_{net} \equiv Q_{ent} - Q_{rec} = Q_{in}. \tag{2}$$

The detailed mechanisms behind entrainment and re-coalescence are not yet fully understood (Dukler and Fabre, 1992). In particular the mechanism by which small bubbles are torn off from the Taylor bubble, i.e. the entrainment process, remains unclear. Delfos (1996) has suggested that the entrainment occurs due to the fact that the liquid interface at the bottom of the Taylor bubble is not able to follow variations in thickness of the downward falling liquid film. Based on this hypothesis he has proposed a model for the entrainment flux. This model is dependent on the velocity of the waves on the film surface, the wave height, the film thickness and the circumference of the tube. Given the uncertainties in the entrainment process and the role of the falling liquid film in this process, our objective here is to measure the characteristics of this falling film and validate the entrainment model according to Delfos (1996). For this purpose we developed a non-intrusive method to measure the film thickness based on a Laser Induced Fluorescence (LIF) technique.

The paper is organised as follows. Some theory of the entrainment model and the falling film is explained in Section 2. The experimental set-up as well as the measurement method are described in Section 3. The results are presented and discussed in Section 4. In the last section conclusions are drawn.

2. Entrainment model

Entrainment is the process of gas loss from the rear of a Taylor bubble, which results in small gas bubbles in the liquid slug.

This entrainment process can be compared to a similar process occurring in case of a plunging jet, i.e. a jet falling into a stationary pool of liquid. Lin and Donnely (1966) and McCarthy et al. (1970) discuss that the disturbances on the jet surface are responsible for the air entrainment. McKeogh and Ervine (1981) state that, in case of a turbulent jet with a very rough surface, the whole gas layer between the most protruding surface structures is carried into the pool.

The above mentioned ideas are applied by Delfos (1996) to the case we study here, i.e. a film surrounding the Taylor bubble. He assumes that perturbations on the falling film surface are responsible for the air entrainment, similar to the case of turbulent plunging jets. The first step in the entrainment process is a transition from a smooth to a rough free surface of the falling liquid film along the Taylor bubble. It was observed that only after these roughnesses or waves appeared on the free surface, gas entrainment increased perceptibly. This led to his conclusion: "entrainment is supposed to be caused by the fact that the free surface of the pool is not capable of responding to the (transverse) oscillations of the incoming film". This process is schematically illustrated in Fig. 2.

The main aspects of this entrainment mechanism can be described as follows. When a wave on the film surface approaches the pool it generates a gravity wave, which propagates on the pool surface (Fig. 2a). When the slope of the induced gravity wave is large enough and the waves on the film surface travel fast enough, the crest of the gravity wave will contact the next wave on the film surface and air will be enclosed (Fig. 2b).

Delfos proposed an expression for the entrainment flux based on parameters as shown in Fig. 3. To simplify the problem, the waves on the film surface are taken sinusoidal with wavelength λ and wave height h_w. The mean film thickness is h_f. The mean velocity of the film is U_f and the velocity of the waves on the surface of the film U_w. The shaded area in Fig. 3 is assumed to be the

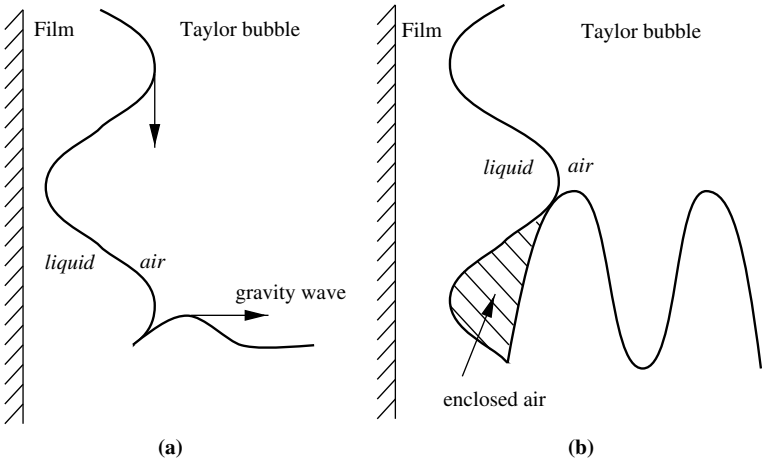

Fig. 2. Entrainment mechanism at the bottom of the Taylor bubble due to distortions on the falling liquid film.

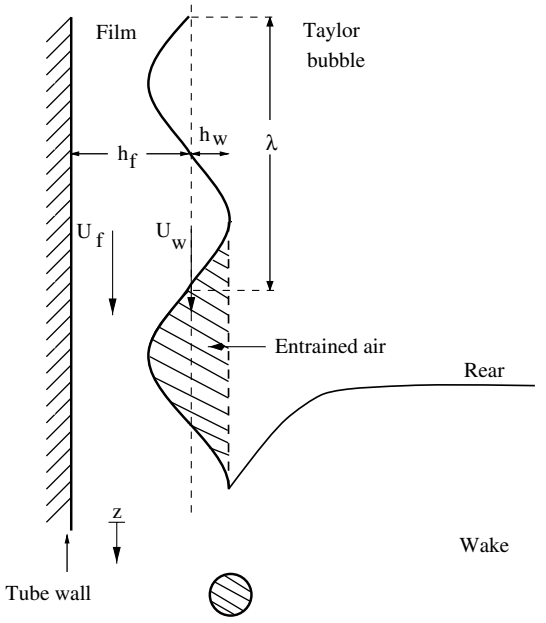

Fig. 3. A schematic picture of the falling film with waves. The shaded area is assumed to be the entrained air.

entrained air. The expression for the entrainment rate, assuming the whole area between the crest of the waves is entrained, then becomes

$$Q_{\text{ent}} = IU_{\text{w}}h_{\text{w}}\pi(D - 2h_{\text{f}}), \tag{3}$$

with I the intermittency factor, which is the fraction of time that disturbances occur at one point on the free surface of the falling film. We approximate U_{w} by means of the wave celerity as measured by Chu (1973) and modelled by Brauner (1987). If we extrapolate their results for our case ($Re = 35 \times 10^3$), the wave celerity will be about 1.2 times the mean film velocity, thus

$$U_{\text{w}} \approx 1.2U_{\text{f}}. \tag{4}$$

The liquid flow surrounding the Taylor bubble is assumed stationary, hence the film thickness $h_{\text{f}}(z)$ relates to the average film velocity $U_{\text{f}}(z)$ following from conservation of mass, i.e. the downward liquid flow rate above the Taylor bubble is equal to the liquid flow rate in the falling film at any location z downstream of the Taylor bubble nose as defined in Fig. 3:

$$Q_{\text{l}} = \frac{\pi}{4}D^2U_{\text{l}} = \frac{\pi}{4}(D^2 - [D - 2h_{\text{f}}(z)]^2)U_{\text{f}}(z), \tag{5}$$

where U_{l} is the downward liquid velocity above the stationary Taylor bubble.

For a thin film ($h_{\text{f}} \ll D$), as is a very good assumption for $z > D$, we can approximate the flow as a two-dimensional film flowing along a flat vertical plate. Then the liquid film velocity, using Eq. (5), linearises to

$$U_{\text{f}}(z) = \frac{DU_{\text{l}}}{4h_{\text{f}}(z)}. \tag{6}$$

Combining Eqs. (3)–(6) and again assuming that $h_f \ll D$, we obtain the following expression for the entrainment flux

$$Q_{ent} = 1.2 Q_l I \frac{h_w}{h_f}. \tag{7}$$

To verify this modelled entrainment flux, we thus have to measure the intermittency factor, the mean film velocity and the average wave height of the waves on the liquid film. The liquid flux, Q_l, is a known and fixed parameter during the measurements.

3. Experiment

3.1. Experimental set-up

The experimental set-up that we have used is described in Delfos et al. (2001b); more details can be found in Delfos (1996). Here we will summarise only the main characteristics. A schematic lay-out of the experimental set-up is illustrated in Fig. 4. It consists of a vertical, cylindrical pipe made

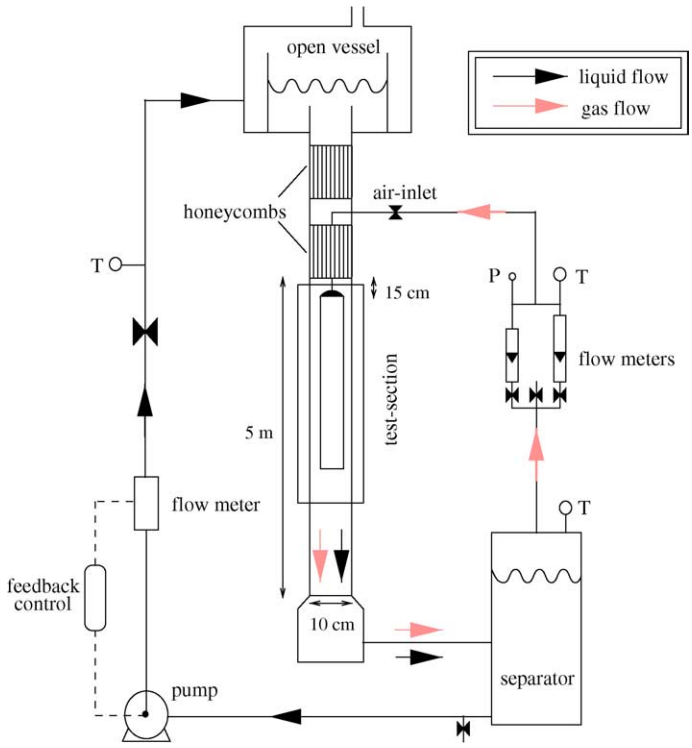

Fig. 4. A schematic drawing of the experimental set-up. The air inlet, Q_{in} at the top of the Taylor bubble is by means of a ROTA flow meter. P and T are measuring points of the pressure and the temperature respectively.

out of perspex with an inner diameter D_i of 100 mm. In this tube a Taylor bubble is generated by continuous injection of air, Q_{in}, through a small tube with tube diameter D_t of 7 mm. At the end of this tube a spherical cap is attached. The purpose of this cap is to stabilise the bubble in the centre of the main vertical pipe. The radius of curvature of this cap, $R_n = 36$ mm, is the same as that of the nose of a theoretical Taylor bubble as found by Dumitrescu (1943).

The bubble is kept at a fixed position by a constant water flow, Q_l, moving downward with a liquid velocity U_l. This liquid velocity is equal to the rise velocity of a Taylor bubble in a stagnant liquid, $U_{tb} = 0.35\sqrt{gD}$ (Dumitrescu, 1943). Above the Taylor bubble a flow straightener (honeycomb) is placed to obtain a uniform velocity profile, and reduce the turbulence in the flow approaching the Taylor bubble. Such a profile is representative for flow conditions encountered by a rising Taylor bubble in a stagnant liquid. Measured velocity profiles were presented in Delfos et al. (2001b). The part of the pipe where the Taylor bubble can be observed is called the test section. This section is enclosed by a rectangular water-filled box to provide a good optical access.

3.2. Entrainment flux measurement

The entrainment flux, using Eq. (2), can be expressed as follows

$$Q_{ent} = Q_{in} + Q_{rec} = Q_{net} + Q_{rec}. \tag{8}$$

To measure the entrainment flux we thus have to measure the gas flow rate into the Taylor bubble and the re-coalescence flux back into the Taylor bubble.

The gas flow rate, Q_{in}, is measured directly with a ROTA-meter as described in Section 3.1. The re-coalescence flux is measured indirectly with a helium injection technique. This technique is described by Delfos et al. (2001a) and in more detail by Kockx (1999), and can be summarised as follows: To the unknown entrainment gas flow rate Q_{ent}, a known flow rate of helium Q_{He} is added, by injecting helium bubbles of similar size as the entrained bubbles in the wake of the Taylor bubble. The proper location to inject the helium bubbles into the wake is described in the paper.

If re-coalescence occurs, helium will enter the Taylor bubble and in case of stationary flow conditions, a constant helium concentration will be established inside the Taylor bubble. By a sample-and-reinjection technique, the helium concentration inside the Taylor bubble, C_{TB}, is monitored continuously. The re-coalescence probability K_{rec}, i.e. the probability that a small gas bubble, after being entrained, coalesces back into the Taylor bubble, is thus a directly measureable quantity: $K_{rec} = Q_{rec}/Q_{ent} = C_{TB}\cdot(Q_{in} + Q_{He})/Q_{He}$. Then, from the mass balance follows that $Q_{ent} = Q_{in}/(1 - K)$.

3.3. Experimental technique to measure the film thickness

To measure the instantaneous liquid film thickness at a given location we need a one-point measurement method, which is able to measure the film thickness continuously with a high sample frequency. Several methods are available to perform such measurements, with as example conductive or needle contact probes. The disadvantage of these techniques is that the probes disturb the flow and the needle point probe measurement is relatively slow. A disturbance of the film flow should be avoided, because it can change the characteristics of the film. Furthermore, the film

thickness in our case has to be measured at various axial positions along the Taylor bubble. This is more complicated to carry out with probes, because many holes in the wall are needed. Another method to measure the film thickness is a light absorption method. However, this requires a detector inside the Taylor bubble, which moreover can transverse in axial direction. This is very complicated to realise in our experimental set-up.

As alternative to the methods discussed above, we have chosen a Laser Induced Fluorescence technique (LIF) proposed by Hewitt et al. (1964). The advantage of this technique is that it is non-intrusive and thus does not disturb the flow. In the LIF method that we have applied, we can measure the film thickness with a laser set-up and a detector both at the same side of the tube. A detector inside the Taylor bubble is thus not needed. Furthermore, the axial traversing of this optical system along the tube wall is relatively straightforward. Our method also allows instantaneous observation of the film thickness at a given position. From these measurements we can obtain statistical information, such as the mean and the variance of the film thickness.

The principle of this LIF-technique is illustrated in Fig. 5. The water in the set-up contains a constant concentration of sodium fluorescein, Uranine AP, [$C_{20}H_{14}Na_2O_5$]. A beam of blue light ($\lambda_L = 488\,\text{nm}$ and diameter beam $= 2\,\text{mm}$) from an Argon-ion laser is transmitted into the liquid film via a small circular mirror with a diameter of 3 mm. The power of this laser is 35 mW. The dye excited by the incident beam emits a green fluorescence ($\lambda_F = 515\,\text{nm}$). This green light is observed by an optical system which is positioned at the same side of the vertical pipe as the incoming blue laser light. After passing a positive lens, the green fluorescence is first separated from any reflected blue light by means of a bandpass filter (XM-535 Corion). This filter reduces the blue light intensity by a factor of 10^7 and has a peak transmittance of green light of at least 60%. Subsequently, the fluorescence is focused on a photo-diode by means of a positive second lens. The signal of the photo-diode V_{ph}, which in our case is amplified with a factor 10^3, is proportional to the intensity of the fluorescent light, I_f. The proportional constant, K_{rec}, depends on the detector properties and the fraction of light captured by the detector.

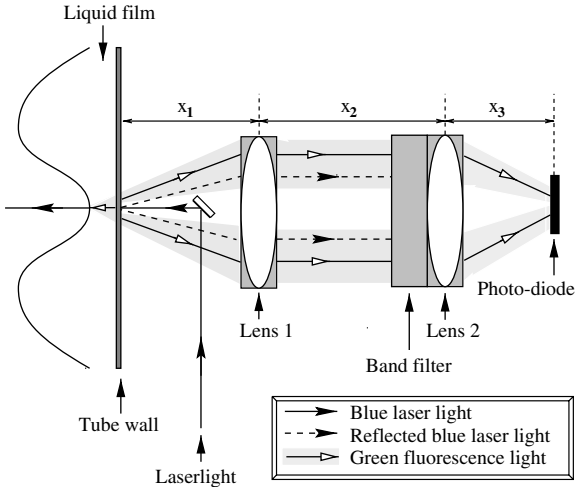

Fig. 5. Schematic figure of film thickness measurement in our experimental set-up with the Laser Induced Fluorescence technique. With $x_1 = 36\,\text{mm}$, $x_2 = 32\,\text{mm}$ and $x_3 = 16\,\text{mm}$.

The intensity of fluorescence depends on the intensity of the incoming blue light I_0, the concentration of the dye C, the film thickness h_f (i.e. the light path through the fluorescence solution) and the properties of the detector (Guilbault, 1973). The relation for the photo-diode signal reads

$$V_{ph} = KI_f = K\Phi I_0(1 - e^{-\epsilon C h_f}), \tag{9}$$

where Φ is the quantum efficiency (0.92 for Uranine AP) and ϵ is the extinction coefficient. During the experiment the concentration of the fluorescent dye and the intensity of the incoming laser light are kept constant. The measured intensity of fluorescence can thus directly be interpreted as a measure for the film thickness. At intermediate concentrations, the fluorescence light is not evenly distributed along the light beam (the exponential term in Eq. (9)), also called the 'inner-cell' effect. Its explanation is that the portion of fluorescence solution nearest to the light source absorbs radiation so that less is available for the rest of the solution. For sufficiently dilute solutions and small film thicknesses this effect gets small and (9) can be simplified to the following relationship

$$V_{ph} = KI_f \approx K\Phi I_0 \epsilon C h_f - \frac{1}{2} K\Phi I_0 \epsilon^2 C^2 h_f^2 + O(h_f^3). \tag{10}$$

The dye concentration in our case is $C = 1 \times 10^{-3}\,\mathrm{g\,l^{-1}}$. It is chosen such that the fluorescence intensity is sufficiently high for the photo-diode to detect but sufficiently low for the inner-cell effect to be not too strong. The laser and the optics are mounted on a traversing system connected to the test-section, such that we can measure at different positions along the Taylor bubble. At every measuring point the intensity of fluorescence as measured by the photo diode is sampled during 15 s with a sample frequency of 4000 Hz.

3.3.1. Calibration

The constant K in the relation between the measured voltage and the film thickness as given in Eq. (10) must be determined by a separate calibration in which the intensity of fluorescence is determined for a set of given film thicknesses. For this we have designed a special calibration set-up (Kockx, 1999), which is shown schematically in Fig. 6.

It consists of a rectangular container, made out of perspex, which is filled with the fluorescent solution. In this container we put a perspex slab, which is shaped more or less in the form of a staircase upside-down, such that between the bottom of the slab and the bottom of the container a set of spaces with a given height is created. At the positions of the well-defined spaces holes are drilled in the staircase shaped slab. These holes are closed on the bottom side with thin glass plates ($d_g = 0.2$ mm). These plates simulate the free surface (water–air) in the experiment. The water–glass–air surface reflects 2.6% more blue light than the water–air surface. At the end of this subsection we discuss how we correct for this extra reflection. Between the glass plates and the bottom of the container a range of liquid layers with well-defined thicknesses between 1.0 and 6.5 mm is created. The expected film thickness is 2.8 mm therefore a range of thickness around this value is chosen. The bottom of the container consists of two perspex walls with a space in between, which is filled with water. This set-up is chosen to imitate the square optical box which surrounds the tube in the experiment. The distances between the optics, the laser and the tube wall is taken the same as in the experiment. During the calibration the fluorescein solution is circulated by a pump to prevent photo-decomposition of the dye.

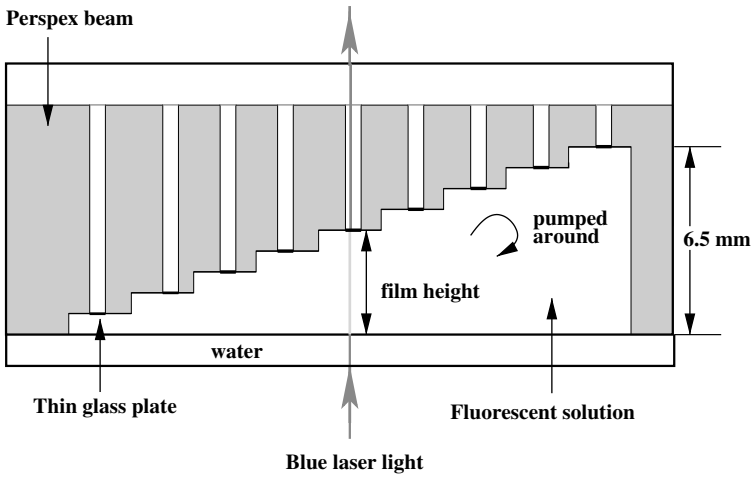

Fig. 6. The calibration set-up.

The fluorescence intensity is now measured for each liquid layer in the calibration cell. During the calibration measurement the following problem was encountered. The voltage, measured by the photo-diode, was found to fluctuate, which could be traced back to the laser. The laser itself fluctuates with 50 Hz and its harmonics. The intensity of this ripple is 2% of the total measured intensity at a given film height. These fluctuations are digitally filtered out when we determine wave height, intermittency and the power spectrum of the film thickness.

In Fig. 7 we show an example of a calibration curve. The measured data are fitted with a second order polynomial (using standard weighted least-squares fitting routines), which agrees with Eq. (10). The inaccuracy in the thickness of the liquid layer is approximately 0.02 mm and the error in the curve fit is 0.5%. If we however perform three separate calibrations in a row (in which each calibration is separately aligned) the error due to three different curve fits becomes 3%, which is also the final error in the calibration.

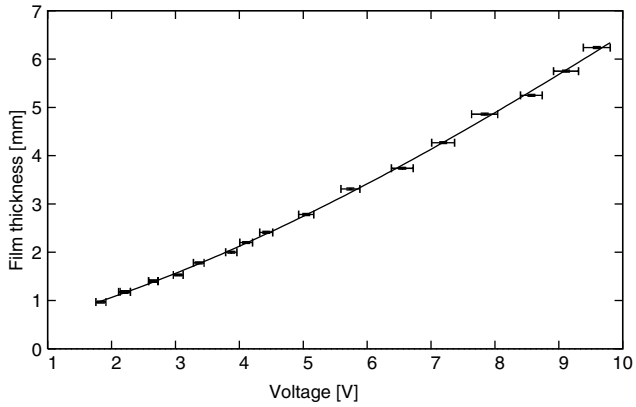

Fig. 7. The calibration curve for the LIF-technique, which gives the relation between film thickness and voltage of the photo-diode (i.e. the fluorescence intensity).

We now have a calibration curve, which is not yet corrected for the extra reflection of blue light at the glass plates. The total intensity of blue laser light, if we take into account the reflection at the glass plates follows as

$$I_l = \int_0^{h_f} I_0 e^{-\epsilon C x}\,dx + \int_0^{h_f} \alpha_g I_0 e^{-\epsilon C h_f} e^{\epsilon C x}\,dx, \tag{11}$$

$$= I_0(1 - e^{-\epsilon C h_f})(1 + \alpha_g e^{-\epsilon C h_f}), \tag{12}$$

$$\approx I_0 \epsilon C(1 + \alpha_g)h_f + \frac{1}{2} I_0 \epsilon^2 C^2 (1 + 3\alpha_g)h_f^2 + O(h_f^3), \tag{13}$$

in which α_g is the total reflection coefficient of blue light at the water–glass–air surface. This results in the following fluorescence intensity measured by the photo-diode

$$V_{ph} = k_{ph} k_A \Phi I_l, \tag{14}$$

$$= A(1 + \alpha_g)h_f + B(1 + 3\alpha_g)h_f^2, \tag{15}$$

in which A and B are unknown constants. To determine A and B we combine Eq. (15) and the second order polynomial ($V_{ph} = c_1 h_f + c_2 h_f^2$) fitted through the calibration data. We can now determine the V_{ph} in case of our experiment (only reflection at the water–air surface) by substituting the reflection coefficient of the water–air surface, α_a, in Eq. (15). To come to an expression for the film thickness as function of the photo-diode signal, $h_f(V_{ph})$, we determine the roots of the corrected second order polynomial.

3.4. Determination of intermittency and wave height

Here we will discuss the procedure to determine the intermittency factor. First we need a method to recognise the undulations present in the instantaneous film thickness signal. This is done in the following way. We calculate the standard deviation over a small time interval, dt, around each data point. In this way we get a kind of contour of the original film thickness signal, as shown in Fig. 8, which we call the local standard deviation signal. We now state that if the local standard deviation signal exceeds a certain threshold value, undulations are present on the film surface. The intermittency factor is then defined as the ratio between the time that the local standard deviation signal exceeds the threshold value (undulation time), T_u, and the total time interval of the time series, T_{tot} (see Fig. 8).

Now that we know the procedure to determine the intermittency factor, we have to define the threshold value and the time interval, dt, over which the local standard deviation is calculated.

In our experiment we have chosen for a time interval, dt, of 2 ms (eight samples). This time interval enables us to detect undulations with a frequency of maximum 500 Hz. This frequency is about the highest frequency present in the power spectrum of the film thickness signal at $L_{tb} > 90$ cm, i.e. Taylor bubble lengths where we observed a rough film surface (Kockx, 1999). A larger dt would not give us information about undulations with high frequencies (of order 100 Hz) and a smaller dt would introduce too much noise.

The threshold value, in other words the noise σ_0, is determined in the following way. We calculate the intermittency with the local standard deviation signal for all kinds of threshold values. In Fig. 9 we show such a 'threshold' graph for three different Taylor bubble lengths, $L_{tb} = 25$, 30

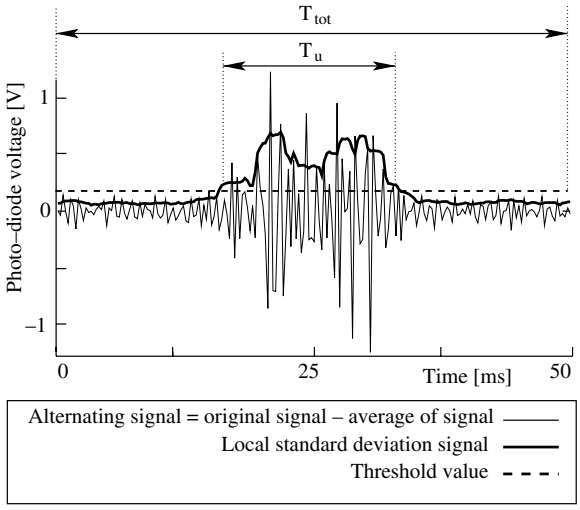

Fig. 8. A model sketch of the alternating film thickness signal (=instanteneous film thickness signal – average film thickness), the local standard deviation signal and the threshold value (=noise). The intermittency, which is defined as the fraction of time that undulations occur on the surface of the falling film is determined by the ratio between T_u and T_{tot}.

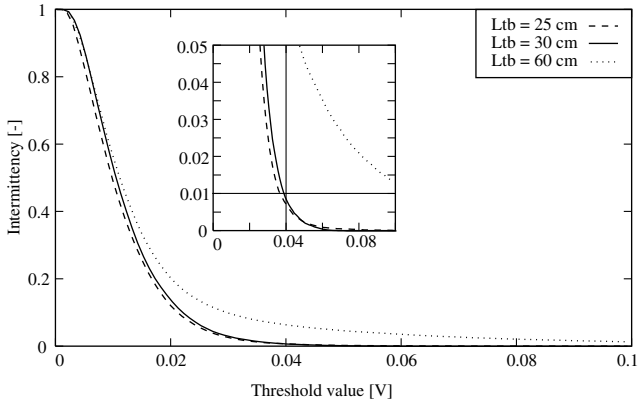

Fig. 9. The graph to determine the threshold value for the intermittency calculation.

and 60 cm. We observe (by eye) that the Taylor bubble surface is 'certainly' smooth at a Taylor bubble length smaller than 30 cm, thus the intermittency at these lengths has to be smaller than (by our definition) 1% (0.01). It then follows, that the threshold value (noise) has to be 0.04 V to satisfy the 1% criterion for short Taylor bubbles. The intermittency factor can now be calculated for all instantaneous film thickness measurements at different L_{tb}, with $\mathrm{d}t = 2$ ms and a threshold value of 0.04 V.

Another parameter needed to calculate the modelled entrainment flux is the wave height of the disturbances on the surface of the falling film. The standard deviation of the interface disturbances that are assumed to contribute to the entrainment, σ_{w}, is obtained from the standard devi-

ation of the filtered film thickness signal σ_{tot} corrected for intermittency I and the threshold value σ_0. This leads to the following expression

$$\sigma_w^2 = \frac{\sigma_{tot}^2 - \sigma_0^2}{I}. \tag{16}$$

If we assume that the disturbances are sinusoidal waves, the wave height becomes

$$h_w \approx \sqrt{2}\sigma_w. \tag{17}$$

4. Results

4.1. Measured entrainment flux

The entrainment flux is measured as described in Section 3.2. First we show the measurement results of net gas flux out of the Taylor bubble, Q_{net} (equal to the gas flow rate into the Taylor bubble, Q_{in}) as a function of Taylor bubble length for stationary conditions. The results, together with the earlier measurements presented in Delfos et al. (2001b), are shown in Fig. 10. The figure shows that there is good agreement, the set-up thus giving consistent results. We see in this figure that Q_{net} is negligible till a Taylor bubble length of about 40 cm ($4D$), this implies that the entrainment flux is equal to the re-coalescence flux or that both fluxes are zero. After this point Q_{net} increases more or less linearly with increasing Taylor bubble length until $L_{tb} = 100\,\text{cm}$ ($10D$). The net gas flux out then reaches a maximum of $0.3751\,\text{s}^{-1}$ at about $L_{tb} = 110\,\text{cm}$ ($11D$) and after this length Q_{net} decreases slowly to a value of about $0.351\,\text{s}^{-1}$ at $L_{tb} = 165\,\text{cm}$ ($16.5D$).

The re-coalescence flux measured by Delfos et al. (2001a) is shown in Fig. 11. We see that the re-coalescence flux is small at $L_{tb} = 51\,\text{cm}$ ($5.1D$) and increases to $0.28\,\text{ls}^{-1}$ at $L_{tb} = 91\,\text{cm}$ ($9.1D$). This is related to the fact that in this range of film lengths, the re-coalsecence probability K_{rec} rises from about 10% for short bubbles to nearly 50% for the largest stable Taylor bubbles.

The measured entrainment flux (the sum of net gas flux and re-coalescence flux) as shown in Fig. 11 is also small at $L_{tb} = 51\,\text{cm}$ ($5.1D$) and increases to a value of $0.60\,\text{ls}^{-1}$ at $L_{tb} = 91\,\text{cm}$

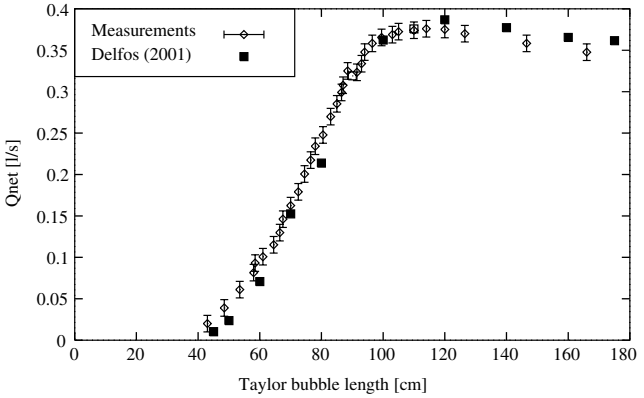

Fig. 10. The net gas flux out (or the gas influx) as function of the Taylor bubble length.

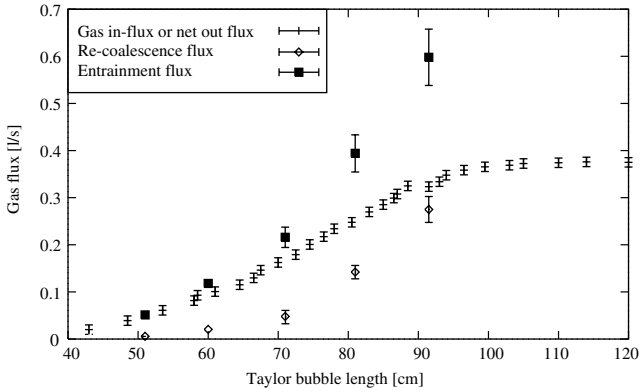

Fig. 11. The measured re-coalescence flux, net gas flux out and entrainment flux as function of the Taylor bubble length.

(9.1D). Unfortunately we do not have separate measurements for the re-coalescence flux (and thus the entrainment flux) beyond $L_{tb} > 91$ cm (9.1D). The net gas flux out of the rear of the Taylor bubble (see Fig. 11), however becomes more or less constant at $L_{tb} > 100$ cm (10D). This means that the difference between the entrainment and re-coalescence flux has become constant at $L_{tb} > 100$ cm (10D).

Measurements on stationary bubbles in a tube were presented by Su (1995), Bacon et al. (1995) and Riiser et al. (1992). However, none of these authors could take into account the re-coalescence flux. Therefore, their entrainment flux measurements are actually measurements of the net gas flux out of the Taylor bubble. Although qualitatively, these authors find characteristics of the net gas loss similar to our results, we will not further consider these for a quantitative comparison on the entrainment flux, since information on both the film characteristics as well as on the coalescence in their experiments is too limited.

4.2. Film thickness

In Fig. 12 we show the measured mean film thickness, h_f, as a function of the distance along a Taylor bubble of 150 cm (15D) length at $Q_{in} = 0.35$ ls^{-1}. The measurement errors as estimated from the calibration inaccuracy are indicated by error bars. The measurements start at a distance of 10 cm (1D) below the nose of the Taylor bubble. More near the bubble nose the 2-D film approximation is not valid any more, and also the film thickness here is outside our calibration range. Fig. 12 shows that the film thickness decreases till 2.6 mm at a distance of 0.8–0.9 m (8–9D). Beyond that region the thickness increases gradually to reach a value of about 2.8 mm for a distance larger than 120 cm (12D). This film thickness agrees with the empirical correlation by Karapantsios and Karabelas (1995), as given in Eq. (A.5), for a fully developed turbulent free-falling film at our $Re = 3.5 \times 10^4$. It also agrees reasonably well with measurements by Su (1995), who found a mean thickness of 3 mm for the liquid film along a Taylor bubble similar to ours at the same Re.

Mean film thickness measurements done with the same liquid flow rate but with other gas influxes ($Q_{in} = 0-0.43$ ls^{-1}), in other words different Taylor bubble lengths, gave the same results as

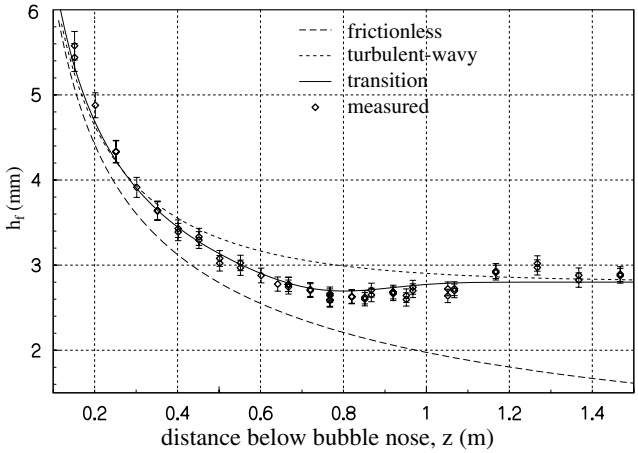

Fig. 12. Mean film thickness as a function of distance below the Taylor bubble nose. Model curves as derived in Appendix A.

the measurements shown in Fig. 12. Thus the development of film thickness is independent of the gas flux into the Taylor bubble in our range of gas in-fluxes, as could be expected from the negligably small stresses at the gas-liquid interface. Therefore we will further assume that the distance z along the Taylor bubble of 150 cm ($15D$) is equivalent to different Taylor bubble lengths and refer to this distance with L_{tb}.

In Fig. 12 we also show three models for the wall film thickness, as they are developed in Appendix A. The first (broken line) is found from a frictionless free falling film, as derived from potential flow theory. The second curve (dotted) is found from a film that is turbulent wavy from the beginning. The third curve (full line) is based on the more elaborate transition model, in which the film starts with a laminar boundary layer at the tube wall, but on its way undergoes transition to a turbulent wavy flow. Here for the intermittency, i.e. the fraction of time that the film is turbulent wavy, we have used the measured intermittency as it will be discussed in the next subsection.

The figure clearly shows that the measurements agree relatively well with the transition model, whereas both others are relatively far off. The minimum in film thickness as it is measured now can be understood from the transition model: There it is assumed that before the transition to a wavy-interface flow occurs the film is still laminar. Because the friction then is very low, the film tends to be stretched very thin. When transition occurs, the friction increases considerably, hence the film thickness increases again. Beyond $L_{tb} > 1.2$ m ($12D$) when film transition has completed, the film reaches both in model and in experiment a more or less constant thickness of 2.8 ± 0.2 mm. From these results, we can conclude that the model with a laminar boundary layer and a gradual transition gives the best description of the film thickness development.

4.3. Intermittency distribution and wave height

The intermittency factor can be determined from the instantaneous film thickness signal by estimating the fraction of time that the signal RMS exceeds a threshold value. Fig. 13 shows the

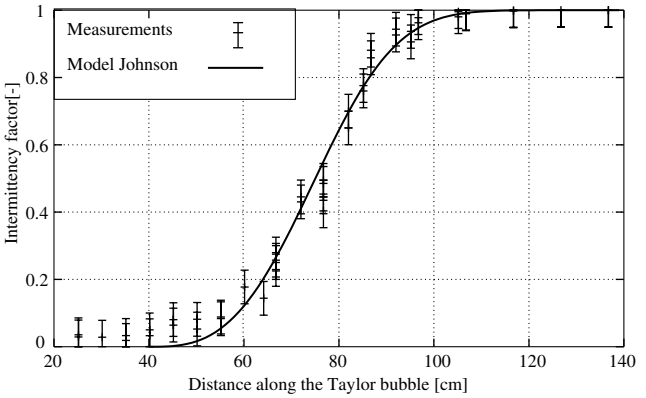

Fig. 13. Measured intermittency distribution along the Taylor bubble at $U_{SL} = 0.35\,\mathrm{ms}^{-1}$ compared with the empirical model by Johnson and Fashifar (1994) for the intermittency distribution of turbulent spots in a boundary layer on a flat plate.

measurements of this intermittency factor, including error bars, along the Taylor bubble, at $U_{SL} = 0.35\,\mathrm{ms}^{-1}$. We see that the intermittency is very low until the bubble reaches a length of 45 cm (4.5D), which is equal to the onset of entrainment discussed in Section 4.1. Beyond this onset of entrainment the intermittency factor grows rapidly to a value of 1 at a Taylor bubble length of 1 m (10D).

In the same figure the intermittency of the surface of the falling film is compared with a model for the intermittency distribution in a boundary layer during transition. In this latter case the intermittency is equal to the percentage of time that turbulent spots occur in the boundary layer (Johnson and Fashifar, 1994). Based on this model their empirical intermittency distribution of turbulent spots reads

$$I = 1 - \exp(-0.0941\xi^3), \tag{18}$$

$$\text{with} \quad \xi = \frac{L_x - L_{on}}{L_{I=0.75} - L_{I=0.25}}. \tag{19}$$

In this expression the onset length, L_{on}, $L_{I=0.75}$ and $L_{I=0.25}$, were determined from a fit to our intermittency data. The values are respectively: 46.2, 85.0 and 67.4 cm. The result is shown as a curve in Fig. 13. The model of Johnson and Fashifar (1994) fits well with our measurements. We can conclude that the increase of intermittency (percentage of waves) on the surface of the falling film shows a similar behaviour as the growth of turbulent spots in a boundary layer.

In Fig. 14 we show the results for h_w along the Taylor bubble. It can be seen that the mean wave height starts with a value of about 0.8 mm and increases to a value of 1.7 mm at $L_{tb} = 1.5$ m (15D). The latter value compares reasonably well with the mean wave height found by Chu (1973) and Zabaras (1985) if we extrapolate their results to our Reynolds number of 3.5×10^4.

The characteristics of the waves can be found from the spectrum of the instantaneous film thickness. The power spectrum of the film thickness signal is shown in Fig. 15 for four different distances along the Taylor bubble: 15, 55, 95 and 137 cm (1.5D, 5.5D, 9.5D and 13.7D), respec-

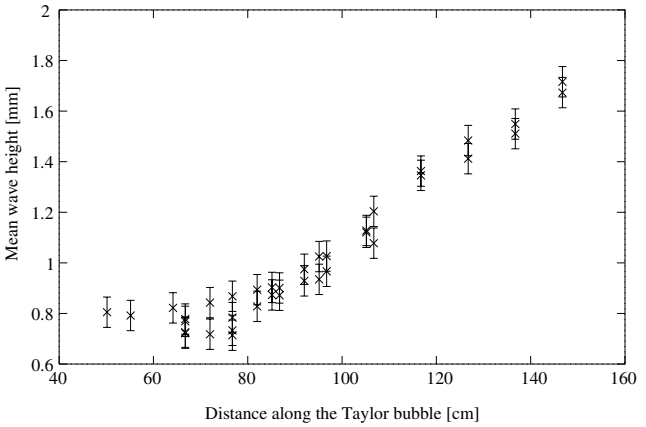

Fig. 14. The mean wave height as a function of distance along the Taylor bubble, assuming the undulations are sinusoidal waves.

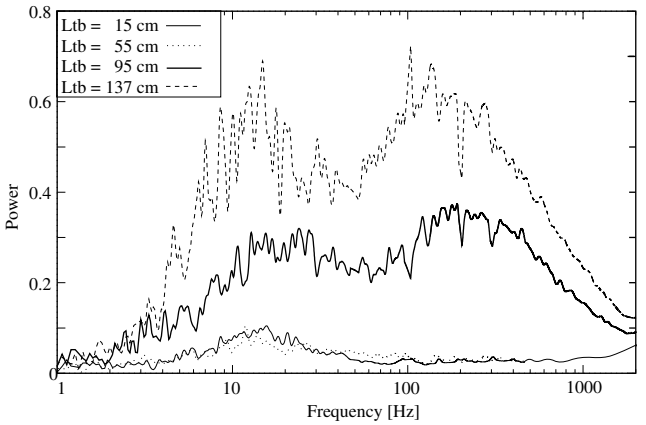

Fig. 15. The power spectrum at four distances along the Taylor bubble: 15 (1.5D), 55 (5.5D), 95 (9.5D) and 137 cm (13.7D).

tively. It follows that for the small distances, i.e. $L_{tb} = 15$ cm (1.5D), the energy of the waves is low. There is only a small peak at about 15 Hz. Thereafter the energy of the waves increases rapidly with increasing distance along the Taylor bubble. At higher Taylor bubble lengths two maxima are found in the spectrum. The first maximum lies at about 15 Hz and the second at about 200 Hz. At $L_{tb} > 1$ m (10D) the spectra are more or less similar. At these Taylor bubble lengths the intermittency is 1 and thus the whole surface can be considered as rough.

The frequency of the long waves agrees more or less with the frequency of 12 Hz for roll-waves, found by Chu (1973) and Zabaras (1985), for free falling film at Reynolds numbers between 200–8000. We can conclude that the long waves present in our measurements behave as roll-waves. In our case, however, there are also short waves present on top of the long wave. These short waves are probably caused by the turbulent eddies in the film. We can give a rough estimate of the wave lengths by means of the frequency and the wave velocity. The wave velocity is determined with

$U_f = 3\,ms^{-1}$ (the average film velocity at $h_f = 2.8\,mm$) using Eq. (4). Ignoring aliasing due to wave vector orientation, this leads to a wave length of about $\lambda_{lw} \approx 24\,cm$ at $f = 15\,Hz$ for the long waves and $\lambda_{sw} \approx 1.5\,cm$ at $f = 200\,Hz$ for the short waves.

4.4. Entrainment model results

The modelled entrainment flux, as found by substituting the intermittency, the wave height, the film thickness and the constant liquid flowrate in Eq. (7), is shown in Fig. 16. In this figure we can see that the modelled entrainment flux is zero till a length of 0.45 m (4.5D), the so-called 'onset of entrainment point' and then the entrainment flux increases till a value of about $1.51s^{-1}$ at $L_{tb} = 1.5\,m$ (15D). At $L_{tb} > 1.2\,m$ (12D) the intermittency, film thickness and mean film velocity have become constant. Thus after this length the entrainment flux only increases due to the increasing wave height.

In the same figure we compare the modelled entrainment flux with the measured entrainment flux (see Fig. 11). It can be seen that the modelled entrainment flux agrees very well with the measured entrainment flux till a length of 1 m (10D). After this length we do not have entrainment flux measurements. This good agreement gives confidence in the entrainment flux proposed by Delfos (1996). According to the model the gas entrainment keeps on increasing when the Taylor bubble becomes longer than the length of 10D at which the net gas flux becomes constant (as shown in Fig. 10). This is due to the fact that the wave height keeps on increasing when the Taylor bubble increases in length (Fig. 14). Apparently, the additional gas entrained at these conditions completely re-coalesces into the rear of the Taylor bubble. Measurements of the re-coalescence probability in the wake show that it strongly increases with increasing gas volume fraction in the wake: At a Taylor bubble length of 91 cm (9.1D), already 45% of the entrained air re-coalesces back into the Taylor bubble. If this result is extrapolated to even higher entrainment rates, one may expect a further increase of re-coalescence probability, which eventually may lead to a net gas loss that decreases with increasing gas entrainment rate. Unfortunately, the measuring technique as applied in Delfos et al. (2001a) was not applicable at higher Taylor bubble lengths.

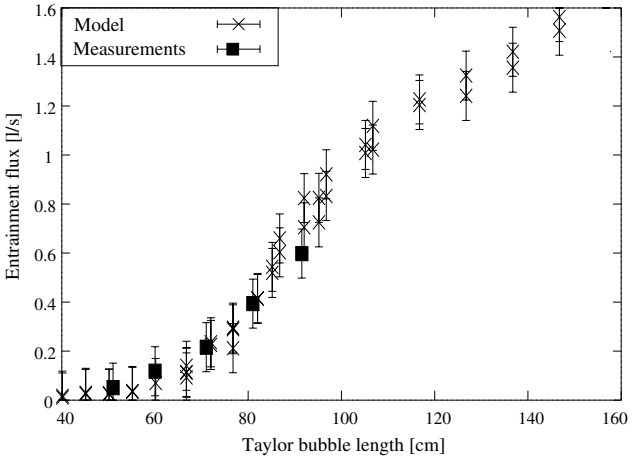

Fig. 16. The modelled entrainment flux compared with the measured entrainment flux.

Such mechanisms are speculative however. Therefore to answer these questions, more data on the film evolution at an even higher L_{tb} as well as re-coalescence data at higher wake void fractions are needed. Furthermore, more advanced measuring techniques suitable for use in the optically dense wake region might give more insight in the physics of the re-coalescence probability.

5. Conclusions

For air/water flow in a vertical tube with a diameter D of 0.1 m we have studied experimentally the gas entrainment at the rear of a Taylor bubble, that was held stationary. Around this Taylor bubble water is flowing in a thin film at a fixed rate. According to a model published earlier the gas entrainment at these conditions depends on the liquid film characteristics. It is proportional to the waviness of the film (its intermittency) and the wave height and inversely proportional to the film thickness. We have measured these film characteristics with a Laser Induced Fluorescence technique for Taylor bubble lengths ranging from $4D$ to $15D$. The gas entrainment at the rear of the Taylor Bubble was determined from the net gas flux into the liquid column underneath it and the rate of entrained gas that re-coalesces. Due to limitations in the latter measuring technique, these measurements only span a Taylor bubble range from $1D$ to $9D$. The results can be summarised as follows:

- The film intermittency becomes non-zero at a Taylor bubble length of $4.5D$ and reaches its maximum value of 1 at $L_{tb} = 10D$.
- The film thickness reaches a constant value of 2.8 mm at $L_{tb} = 12D$.
- The height of waves at the film surface increases as the Taylor bubble length increases. Although the constant average film thickness for $L_{tb} > 12D$ suggests a fully developed film flow, the further increasing wave height suggests that a fully developed state is still not reached at $L_{tb} = 15D$.
- Gas entrainment starts to occur at $L_{tb} = 4.5D$, i.e. when the first waves appear. For values of the Taylor bubble lengths up to $9D$ the measurements compare very well with the model results, when measured film data are subsituted in the equation. For $L_{tb} = 9D$–$15D$ the model indicates that the gas entrainment keeps on increasing with Taylor bubble length.
- The net gas flux into the liquid column underneath the Taylor bubble is also an increasing function of its length. However it reaches a constant value at $L_{tb} = 10D$. Apparently beyond that point any additional entrained gas completely re-coalesces with the Taylor bubble. A study of the reason why this occurs will require more data of the kind we have presented here and in Delfos et al. (2001a), as well as more powerful diagnostic tools, capable of being used in the high void fraction wake region.

Acknowledgments

The authors thank T.D. Tujeehut and J.L.J. Zijl for their work on the experimental part of this research.

Appendix A

Here we will briefly describe a model for the thickness of the liquid film surrounding the Taylor bubble, i.e. the liquid film flowing down along the tube wall. In our laboratory experiment, the Taylor bubble is fixed at a constant axial position. Thus in the laboratory reference frame, the film flow is stationary downward along a non-moving wall. This implies that the shear stress inside the film is dominated by the wall induced stress, whereas the shear stress at the water–air interface can be neglected. We can also assume the flow to be stationary, i.e. except for waves on the interface the film height is constant in time. Then the film thickness $h_f(z)$ relates to the average film velocity $U_f(z)$ following from conservation of mass, i.e. the downward liquid flow rate above the Taylor bubble is equal to the liquid flow rate in the falling film at any location z downstream of the Taylor bubble nose as defined in Fig. 17:

$$Q_l = \frac{\pi}{4} D^2 U_l = \frac{\pi}{4} (D^2 - [D - 2h_f(z)]^2) U_f(z), \tag{A.1}$$

where U_l is the downward liquid velocity above the stationary Taylor bubble. Thus we find for the film thickness $h_f(z)$:

$$h_f(z) = \frac{D}{2} \left(1 - \sqrt{1 - \frac{U_l}{U_f(z)}} \right). \tag{A.2}$$

For a thin film ($h_f \ll D$), as is a very good assumption for $z > D$, we can approximate the flow as a two-dimensional film flowing along a flat vertical plate. Then the film thickness linearises to:

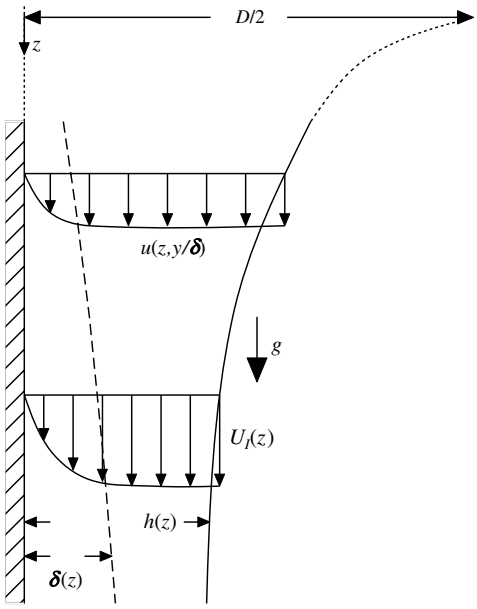

Fig. 17. Boundary layer developing in the falling liquid film along the tube wall.

$$h_f(z) \approx \frac{DU_l}{4U_f(z)}, \tag{A.3}$$

which we will use further on. In order of appearance, we will now describe (i) the final stage, (ii) the initial stage, and (iii) the intermediate stage of the film flow.

(i) After development effects at the inlet, a liquid film flow will eventually reach a fully developed state. The state depends on the hydraulic Reynolds number, $Re_H = 4U_f(z)h(z)/v = U_lD/v$ where the mass balance was used. Since we only consider relatively high values (in the experiment $Re_H \approx 3.5 \times 10^4$), the final state of our film is highly turbulent, with large amplitude roll waves (Karapantsios and Karabelas, 1995; Brauner, 1987). For the present modelling, we are only interested in the mean film thickness, h_{ftw}. For flow over a smooth wall, we find applying the Blasius friction factor,

$$h_f = 0.135\left(\frac{v^2}{g}\right)^{\frac{1}{3}} Re^{\frac{7}{12}}. \tag{A.4}$$

For our case this leads to a thickness of the equilibrium turbulent film equal to 2.8 mm. If we use the correlation by Karapantsios and Karabelas (1995), who obtained data in the range of $Re_H = (500–13{,}000)$:

$$h_{ftw} = 0.214\left(\frac{v^2}{g}\right)^{\frac{1}{3}} Re^{0.538}, \tag{A.5}$$

which gives 2.8 mm as well, which is further confirmed within 10% by older data (Belkin et al., 1959) for $Re_H = (5000–30{,}000)$. From the mean film thickness, we easily find a fully developed film velocity, U_{fFD} from the mass balance.

(ii) Compared to the final thickness of the film of a few mm, the initial thickness of 50 mm (half the tube diameter) is much larger. Thus we can expect that the film is far from fully developed near the Taylor bubble nose. Since we consider high Reynolds number film flow only, we can first consider the flow as inviscid, i.e. frictionless. Then applying Bernoulli's law to the free surface streamline starting from the stagnation point at the nose of the bubble, we find for the interface velocity of the film, U_i:

$$U_i = \sqrt{2gz}. \tag{A.6}$$

In the inviscid flow, the velocity profile in the film quickly gets flat after the curved part near the bubble nose, i.e. for $z > D$. Thus the inviscid film thickness $h_{fi}(z)$ is found from the mass balance:

$$h_{fi}(z) = \frac{DU_l}{4\sqrt{2gz}}. \tag{A.7}$$

Thus we see that the film quickly gets thinner. At $1D$, it has already shrunk to a mere 6 mm. The state of the flow, either laminar or turbulent, does not have any influence on this initial phase.

(iii) Let us now consider the change from the initial free-fall to the finally fully developed turbulent wavy flow. If we assume the flow to be turbulent from the beginning, we can take the friction factor of the film as a constant, in which the equation of motion for the film can be written as (Delfos, 1996):

$$\frac{\mathrm{d}}{\mathrm{d}z}\frac{1}{2}U_{\mathrm{f}}^2 = g\left(1-\left(\frac{U_{\mathrm{f}}}{U_{\mathrm{fFD}}}\right)^3\right), \tag{A.8}$$

where the inverse function $z(U_{\mathrm{f}})$ can be solved analytically:

$$z\left(U_{\mathrm{f}}^{FD}\right)g/U_{\mathrm{fFD}}^2 = \frac{1}{6}\ln\left(1+U_{\mathrm{f}}^{FD}+U_{\mathrm{f}}^{FD^2}\right)-\frac{1}{3}\ln\left(1-U_{\mathrm{f}}^{FD}\right)-\frac{1}{\sqrt{3}}\left(a\tan\left(1+2U_{\mathrm{f}}^{FD}/\sqrt{3}\right)-\pi/6\right) \tag{A.9}$$

with $U_{\mathrm{f}}^{FD} = U_{\mathrm{f}}/U_{\mathrm{fFD}}$ the non-dimensional film velocity. The resulting film thickness is plotted in Fig. 12.

In Section 4.2 we show that this 'fully turbulent' model highly underestimates the thinning of the film. This can be understood from the fact that the film flow is more likely to be laminar from the beginning: not only is turbulence in the flow upstream of the bubble nose reduced by a honeycomb flow straightener, but also in the accelerational phase of the film, turbulence is further reduced or even suppressed (Loehrke and Nagib, 1976).Therefore, it is more likely that at the tube wall a laminar boundary layer will form itself. In principle, this boundary layer will develop as soon as the liquid flow leaves the honey-comb section. A full treatment of the boundary layer from this point on is yet not that relevant, while the momentum of the whole flow (including that of the boundary layer) is rather low before the nose part of the bubble is reached. Only in the strongly accelerating phase after the bubble nose passage, stresses in this layer are important. The development of the boundary-layer thickness $\delta(z)$ and its displacement thickness $\delta^*(z)$ for the case of a two-dimensional laminar flow with constant acceleration g can be solved straightforward using Pohlhausen's method (Delfos, 1996):

$$\delta(z) = 3.41\sqrt{v\sqrt{\frac{z}{2g}}}, \delta^*(z) \approx 0.252\delta \tag{A.10}$$

with v the kinematic viscosity of the liquid. The accelerating boundary layer causes a non-uniform velocity profile within the film. As a consequence we have to correct the free-falling film thickness (A.2) by adding to h_{fi} the displacement thickness δ^* due to the presence of the boundary layer. Thus we find for the laminar film thickness $h_{\mathrm{fL}}(z)$:

$$h_{\mathrm{fL}}(z) = h_{\mathrm{fi}}(z)+\delta^*(z) = \frac{DU_1}{\sqrt{2gz}}+0.859\sqrt{v\sqrt{\frac{z}{2g}}}. \tag{A.11}$$

The boundary layer growth will proceed until the shear stress is fully developed throughout the whole film height, i.e. when $\delta(z)$ approaches $h_{\mathrm{fi}}(z)$, or until the film flow has become unstable. It can easily be shown that it takes several meters of film drop before the equilibrium film thickness for laminar flow (Nusselt, 1916) is reached. Film flow instability can occur either by transition to a turbulent boundary layer, or to an unstable wavy film interface. In our experiment, we observed the film surface to start having wavy patches already some 0.5 m below the Taylor bubble nose. We can only guess that this wavy interface is initiated by instabilities in the boundary layer, but cannot prove this. Any way, after such a transition the laminar model above is not sufficient any

more. Therefore, we introduce the intermittency $I(z)$, i.e. the fraction of time (or the fraction of tube circumference) at a certain position z that the film is wavy. We now model the average film thickness $\langle h_f(z)\rangle$by simply averaging:

$$\langle h_f(z)\rangle = (1 - I(z))h_{fL}(z) + I(z)h_{fFD}, \tag{A.12}$$

where the intermittency is determined from the experiments, as described in Section 4.3. In Section 4.2 we show that this more elaborate film model reasonably well describes the evolution of film thickness.

References

Bacon, R.P., Scott, D.M., Thorpe, R.B., 1995. Large bubbles attached to spargers in downwards two-phase flow. Int. J. Multiphase Flow 21, 949–959.

Belkin, H.H., MacLeod, A.A., Monrad, C.C., Rothfos, R.R., 1959. Turbulent liquid flow down vertical walls. AIChE J. 5, 245–248.

Brauner, N., 1987. Roll wave celerity and average film thickness in turbulent wavy films. Chem. Eng. Sci. 42, 265–273.

Brauner, N., Barnea, D., 1985. Holdup of the liquid slug in two-phase intermittent flow. Int. J. Multiphase Flow 11, 43–49.

Chu, K.J., 1973. Statistical characterization and modelling of wavy liquid films in vertical two-phase flow. Ph.D. thesis, University of Houston, Texas.

Delfos, R., 1996. Experiments on air entrainment from a stationary slug bubble in a vertical tube. Ph.D. thesis, Delft University of Technology.

Delfos, R., Rops, C.M., Kockx, J.P., Nieuwstadt, F.T.M., 2001a. Measurements of the recoalescence flux into the rear of a Taylor bubble. Phys. Fluids 13, 1141–1150.

Delfos, R., Wisse, C.J., Oliemans, R.V.A., 2001b. Measurements of air entrainment from a stationary Taylor bubble in a vertical tube. Int. J. Multiphase flow 27, 1769–1787.

Dukler, A.E., Fabre, J., 1992. Gas–liquid slug flow; knots and loose ends. Third Int. Workshop on Two-Phase Fundamentals, ICL.

Dumitrescu, D.T., 1943. Stroemung an einer Luftblase im senkrechten Rohr. Z. Angew. Math. Mech. 23, 139–149.

Fabre, J., Liné, A., 1992. Modeling of two-phase slug flow. Ann. Rev. Fluid Mech. 24, 21–46.

Fernandes, R.C., Semiat, R., Dukler, A.E., 1983. Hydrodynamic model for gas–liquid slug flow in vertical pipes. AIChE J. 29, 981–989.

Guilbault, G.G., 1973. Practical Fluorescence. Marcel Dekker Inc., New York.

Hewitt, G.F., Lovegrove, P.C., Nicholls, B., 1964. Film thickness measurement using fluorescence technique. Atomic Energy Research, Harwell, AERE - R4478.

Johnson, M.W., Fashifar, A., 1994. Statistical properties of turbulent bursts in transitional boundary layers. Int. J. Heat Fluid Flow 15, 283–290.

Karapantsios, T.D., Karabelas, A.J., 1995. Longitudinal characteristics of wavy falling films. Int. J. Multiphase Flow 21, 119–127.

Kockx, J.P., 1999. Gas exchange between a stationary Taylor bubble and its liquid slug in a vertical pipe. Ph.D. thesis, Delft University of Technology.

Lin, T.J., Donnely, H.G., 1966. Gas bubble entrainment by plunging laminar liquid jets. AIChE J. 12, 563–571.

Loehrke, R.I., Nagib, H.M., 1976. Control of free stream turbulence by means of honeycombs. J. Fluid Eng., 342–354.

McCarthy, M.J., Henderson, J., Molloy, N.A., 1970. Entrainment by plunging jets. In: Proc. Chemeca 1970 Conf., Australia, Butterworths, pp. 86–100.

McKeogh, E.J., Ervine, D.A., 1981. Air entrainment rate and diffusion pattern of plunging liquid jets. Chem. Eng. Sci. 36, 1161–1172.

Nusselt, W., 1916. Die Oberflaechenkondensation des. Z. Ver. Dtsch. Ing. 60, 541–546.

Orell, A., Rembrandt, R., 1986. A model for gas–liquid slug flow in vertical tubes. Ind. Eng. Chem. Fundam. 25, 196–206.

Riiser, K., Fabre, J., Suzanne, C., 1992. Gas entrainment at the rear of a Taylor bubble. In: Proc. European Two-Phase Flow Group Meeting, Stockholm.

Shemer, L., Barnea, D., 1989. Void fraction measurements in vertical slug flow: Applications to slug characteristics and transition. Int. J. Multiphase Flow 15, 495–504.

Su, C., 1995. Gas entrainment at the bottom of a Taylor bubble in vertical gas–liquid slug flows. Ph.D. thesis, University of Houston, Texas.

van Hout, R., Barnea, D., Shemer, L., 1992. Spatial distribution of void fraction within a liquid slug and some other related slug parameters. Int. J. Multiphase Flow 18, 83.

Zabaras, G.J., 1985. Studies of vertical gas liquid flows. Ph.D. thesis, University of Houston, Texas.